Supersonic Combustion
Using a Stinger-Shaped Fuel Injector

Toshinori Kouchi[*] and Goro Masuya[†]
Tohoku University, Sendai, Miyagi 980-8579, Japan

Kohshi Hirano[‡] and Akiko Matsuo[§]
Keio University, Yokohama, Kanagawa 223-8522, Japan

and

Sadatake Tomioka[**]
Japan Aerospace Exploration Agency, Kakuda, Miyagi 981-1525, Japan

We developed a stinger-shaped injector (stinger injector) for supersonic combustors in cold-flow experiments. The stinger injector has a port geometry with a sharp leading edge in front of a streamwise slit. This injector produced higher jet penetration at a lower jet-to-crossflow momentum flux ratio (J) than a conventional circular injector. We applied the injector in a Mach 2.44 combustion test at a stagnation temperature of 2060 K. At a low fuel equivalence ratio (Φ) regime (i.e., low J regime), the injector produced 10% higher pressure thrust than the circular injector because of high jet penetration as expected from the cold-flow experiments. Even at a moderate Φ regime, the stinger injector produced higher pressure thrust than the circular injector. At moderate Φ, the stinger injector held the flame around the injector and generated a precombustion shock wave in front of the injector. The presence of the precombustion shock wave decreased the momentum flux of the crossflow air and diminished the advantage of the injector for jet penetration. The injector, however, produced higher pressure thrust because better flame-holding produced higher pressure around the injector. At a higher Φ regime, the precombustion shock wave went upstream with both injectors. The far-upstream presence of a precombustion shock wave increased the

---
[*] Assistant Professor, Department of Aerospace Engineering, Member AIAA.
[†] Professor, Department of Aerospace Engineering, Senior Member AIAA.
[‡] Graduate Student, Department of Mechanical Engineering, Member AIAA.
   Currently, Researcher, Thermal Technology Department, Technical Institute, *Kawasaki Heavy Industries, Ltd.*
[§] Professor, Department of Mechanical Engineering, Senior Member AIAA.
[**] Senior Researcher, Combined Propulsion Research Group, Senior Member AIAA.

turbulence in the crossflow and spread the fuel from both injectors. Thus, the difference in injector shape was insignificant for thrust performance.

Nomenclature

A_{in}	=	area at entrance of combustor
B_i	=	mole fraction of chemical species i in crossflow air
D	=	equivalent diameter or diameter of injection orifice
F	=	pressure thrust
J	=	jet-to-crossflow momentum-flux ratio
P	=	pressure
P_b	=	effective back pressure
R_c	=	local fuel consumption rate
T	=	temperature
S_k	=	relative uncertainty in k element, %
x, y, z	=	stream-, span-, height-wise coordinate
X_i	=	mole fraction of chemical species i ($= N_2, O_2, H_2$) measured by gas chromatography
ΔF	=	increment of pressure integration with combustion
ϕ	=	local fuel equivalence ratio
Φ	=	bulk fuel equivalence ratio
η_c	=	local combustion efficiency

Subscripts

0	=	stagnation condition
A	=	without combustion
C	=	with combustion
$circular$	=	circular case
j	=	injection
psw	=	disturbed crossflow-air with precombustion shock wave
$stinger$	=	stinger case

| W | = | wall |
| ∞ | = | undisturbed crossflow |

I. INTRODUCTION

SCRAMJET engines require rapid mixing and reaction of fuel because of the limited time and length available in the combustor. A major difficulty with the fuel injection system is achieving high penetration of the fuel jet into the high-speed airflow to spread the fuel into the entire combustor area for efficient mixing and combustion. A scramjet combustor with a circular cross-section has a low aspect ratio. Therefore, fuel penetration is a major problem for this type of the combustor. Even for a rectangular scramjet combustor, penetration is a major problem. A rectangular combustor with a high aspect ratio has closely spaced upper and lower walls. Penetration is not an issue for this type of the combustor. However, this type of combustor is not appropriate for high Mach numbers, because it increases the friction drag of the engine and reduces the net thrust [1]. Therefore, the aspect ratio of the combustor will be relatively low and penetration will be a major problem even for a rectangular scramjet combustor. Thus, many fuel injection systems for the scramjet [2] have been designed and investigated to achieve high penetration.

Fuel-injection systems for scramjets are mainly divided into two categories: systems using intrusive devices and systems using non-intrusive devices to promote jet penetration and mixing. The intrusive devices, for example, are ramps [3,4], struts [5] and pylons [6,7]. These devices greatly improve uniformity of fuel distribution in the combustor, but they create intense aerodynamic disturbances with an inevitable increase in total pressure losses and drag. In addition, the devices suffer severe thermal loads. Therefore, the devices usually require active cooling, adding system complexities. The non-intrusive injectors reduce the total pressure loss, compared with intrusive ones. Thus, non-intrusive injectors are more attractive if the systems obtain high jet penetration.

Jet penetration of the non-intrusive, wall-flush-mounted, injectors is dominated mainly by two parameters: jet-to-crossflow momentum flux ratio J (i.e., dynamic pressure ratio) and ratio of injection pressure to effective back pressure (P_b) [8] around the orifice. The jet penetration of fuel injected perpendicularly from a conventional circular injector is proportional to $J^{1/3} \sim J^{1/2}$ [9,10] and is a weak function of J. Therefore, transverse injection using a circular injector requires very high injection pressure to achieve high jet penetration. High injection pressure increases the fuel mass flow rate, and mixing performance tends to decrease with increased fuel mass flow from the

injector. In addition, the engine system imposes limitations on the total mass flow rate of the fuel with each flight condition (e.g., bulk fuel equivalence ratio (Φ) of unity). Therefore, injection pressure cannot increase without limiting high jet penetration.

The non-intrusive methods are classified into three categories: angled injection [10-12], port geometry optimization (elliptical [11,13], wedge [14], or diamond [15-17] shapes), multi-array injection (e.g., aeroramp [18,19], staged [20], and cascade [21,22] injectors), and their combinations. Low-angled injection systems [10,11] and the aeroramp injector [19] exhibited jet penetration trends similar to those of the physical ramp injector. These flush-mounted injectors reduced total pressure loss and prevented severe thermal loads. Such injectors and the physical ramp injector efficiently increase the jet penetration in the far field of the injector, though their penetrations were lower than that using transverse injection. Tandem two-staged injection behind a backward-facing step exhibited that the blockage effect of the upstream jet facilitated the penetration of the downstream jet [20]. A cascade injector [21,22] is a more progressive design actively using the tandem effect to increase the jet penetration. The cascade injector has several flow passes inside the injector, and requires a separated fuel manifold and a control valve for each flow pass, adding system complexities.

Another approach is to optimize fuel-port geometry for achieving effective penetration. Fuel-port geometry significantly affects jet penetration because the plume shape dominates the effective back pressure. A wedge-shaped orifice [14] and a diamond-shaped orifice [15] produced better penetration than the circular injector because they reduced P_b by avoiding the boundary-layer separation ahead of the injector in low J regimes. Recently, Tomioka et al. attempted to further reduce P_b for the diamond-shaped orifice in higher J regimes and introduced a pressure-matched supersonic jet through the diamond-shaped orifice [23]. The injector was proven to achieve low jet-airflow interaction and to promote the jet penetration in a cold-flow experiment using helium injectant. The injector, however, did not improve thrust in combustion tests [24] because of greater ignition delay and lower pressure level near the fuel injector due to the inherently reduced disturbance of the mainstream.

We improved the diamond-shaped injector by another method that does not require pressure-matching and developed a new injector geometry with a very high length-to-width ratio with a sharp leading edge. We refer to this as a stinger-shaped injector [25]. The stinger-shaped injector (stinger injector) greatly reduced P_b around the injector due to its reduced width. Parametric CFD and experiments for optimizing fuel-injector geometry [25] revealed that a

higher length-to-width aspect ratio injector achieves higher jet penetration. In a cold-flow experiment, the stinger injector achieved 60% higher penetration than either the circular or supersonic diamond injectors did [25].

In this study, the stinger injector was tested in a reactive-flow experiment with total temperature of 2060 K (M2.44 supersonic flow). Mixing and combustion characteristics were compared with those using the traditional circular injector. Combustor performance (e.g., thrust, ignition/flame-holding and mode transition point) was also examined. Intensive combustion induces a scramjet-to-dual-mode transition and generates a precombustion shock wave, which decreases crossflow speed and increases ambient pressure around the injectors. These changes may reduce the advantage of the stinger injector, because its penetration is saturated with increasing J. Therefore, this study also discusses the effects of the precombustion shock wave on injector performance.

For a realistic scramjet combustor, fuel injectors will be arrayed in the spanwise direction. However, we used a single-injector configuration. For multi-injector configurations, the mixing and combustion characteristics as well as thrust depends heavily on the spacing between injectors [26]. We should carefully determine the appropriate spacing, because the advantage of the stinger injector could be eliminated by inappropriate spacing. The data of the single-injector configuration will be baseline data for assessing multi-injector configurations. In addition, the data of the single-injector configuration will help us determine the appropriate spacing for the stinger injector. The results of the multi-injector configuration using the stinger injector will be presented in another paper.

II.   EXPERIMENT APPARATUS AND DATA REDUCTION

A. Wind Tunnel

We used a blow-down direct-connect combustor test facility (Fig. 1). The nozzle block assembly provided a Mach 2.44 supersonic flow. Using a hydrogen-fuel vitiation heater, the test gas simulated airflow at a stagnation pressure (P_0) of 1.05 ± 0.02 MPa, a total temperature (T_0) of 2060 ± 60 K, and an oxygen mole fraction of 21.0 ± 1.0 vol.%. The vitiated air contained 26.6 vol.% water vapor. The unit Reynolds number based on these conditions was 6.0×10^6 m^{-1}. The entrance of the combustor was 51-mm high and 94.3-mm wide. The combustor was divided into two sections: a 507 mm-long constant-area section and a 635 mm-long diverging section. The diverging section had a half expansion angle of 1.66°. The combustor was sited in the atmosphere, and the combustion flow was exhausted to atmospheric pressure.

B. Stinger Injector

The combustor was equipped with an injector block assembly on the bottom wall in the constant-area section 376 mm downstream of the nozzle exit. The assembly could be replaced for each test run. Injection pressure (P_j) was monitored in the plenum of the assembly for evaluating J. A sharpened-edge orifice flow meter was installed far upstream of the plenum. It measured the fuel mass flow rate with an accuracy of $\pm$ 3%, for evaluating both the discharge coefficient of injection orifice and Φ.

Hydrogen fuel at room temperature was injected perpendicularly through a sonic orifice on the assembly to the crossflow. Figure 2 depicts the two different injectors used in this study: (a) a conventional circular injector with a 6 mm diameter and (b) a stinger injector with an equivalent diameter of 6 mm. The circular injector yielded baseline data to assess the performance of the stinger injector. The stinger injector had a half angle of 5° in front of a streamwise slit. It was 1.2 mm wide and 27 mm long. The discharge coefficient of the circular injector was 0.83, and that of the stinger injector was 0.79. The stinger injector required 5% higher injection pressure (i.e., momentum-flux ratio) than the circular injector to attain a given Φ. Note that $\Phi \sim 0.2$ corresponded to J of unity.

At a low J, the stinger injector delivered higher jet penetration than the circular injector. Therefore, the stinger injector is expected to produce higher combustor performance at low J. Figure 3 compares the jet penetration of the stinger injector with that of the circular injector, both obtained in a cold-flow experiment using helium injectant. The jet penetration was measured by gas sampling data at 131-mm downstream of the injector. The penetration height (H) was defined as the vertical height from the injection plane to the position where the maximum concentration was detected. The penetration height of the stinger injector was greater than that of the circular injector below $J \sim 3$ and saturated with increasing J. The rapid saturation of H was caused by the axis switching of jet expansion that was the same phenomenon as observed in the experiment using the diamond-shaped orifice [23]. Figure 4 presents back views of the jet plumes through the stinger (right) and circular (left) injectors at $J = 1$ and $J = 4$ obtained by numerical simulation [25] under the same conditions as for the cold-flow experiment. The plume of the stinger injector penetrated deeply in the vertical direction at $J = 1$. Its plume maintained the narrow shape of the orifice. However, the plume of the stinger injector deformed into a V-shape at $J = 4$ due to uneven expansion in the span- and stream-wise directions. The blunt shape of the plume restricted the vertical penetration of the stinger injector. Based on these results, the stinger injector is expected to produce higher combustor performance below $J \sim 3$, corresponding to $\Phi \sim 0.6$.

C. Wall Pressure Measurement

We measured wall pressure (P_W) on both the injector-side wall and the opposite-side wall using two mechanical scanning pressure sensors. We normalized P_W by the measured P_0, to mitigate run-to-run deviation of the stagnation. Uncertainty of the run-to-run deviation was evaluated to be ± 2% of local P_W/P_0, based on seven-run repeatability at a given Φ. Measured data fluctuated slightly during the test; fluctuation in the combustion region was ± 2% of local P_W/P_0. After taking the square root of each element of the uncertainties, the overall uncertainty of the wall-pressure measurement (S_{Pw}) was calculated to be ± 3% of local P_W/P_0.

D. Evaluation of Pressure Gain and Increment of Pressure Integration

We divided the P_W/P_0 distribution of the stinger injector by that of the circular injector to determine the benefit of the stinger injector. We refer to this pressure ratio ($P_{W,stinger}/P_{W,circular}$) as the pressure gain of the stinger injector. The uncertainty of the pressure gain of the stinger injector was ± 4.2%, based on S_{Pw}.

Integration of the P_W distribution in the diverging section yielded pressure thrust (F). We evaluated the thrust increment ($\Delta F = F_C - F_A$) by subtracting F without combustion (F_A) from F with combustion (F_C). The change in friction force due to combustion was ignored in this study. The increment ΔF was normalized by P_0 and the cross-sectional area at the entrance of the combustor (A_{in}). Simple integration of measured P_W overestimated F at the low Φ regime including fuel-off, because the flow separated at the combustor exit. Therefore, an imaginary pressure distribution without separation derived by curve-fitting the P_W distribution upstream of the separation point with Crocco's pressure-area rule of $PA^{\varepsilon/(\varepsilon-1)}$ was used for the integration [27]. $F_A/(P_0 \cdot A_{in})$ was estimated to be 0.034 at fuel-off. The uncertainty in P_W/P_0 yielded the following uncertainty in local ΔF.

$$S_{\Delta F} \quad = \quad S_{Pw}\sqrt{\frac{F_C^2 + F_A^2}{\left(F_C - F_A\right)^2}} \tag{1}$$

E. Gas Sampling Measurement

We sampled gas at the exit of the combustor using a water-cooled sampling probe to evaluate the local equivalence ratio and combustion efficiency. The probe ensured reaction quenching during sampling [28]. There were 63 sampling points with an interval of 10 *mm* (9 points in the height direction x 7 in the width direction). The duration of the sampling was 2.5 *s*, and the diameter of the probe inlet was 0.3 *mm*.

Gas chromatography was used to analyze the sampled gas with an uncertainty of ± 1.0 vol.% for N_2, ± 0.4 vol.% for O_2 and ± 0.6 vol.% for H_2. The sampled gas composition yielded the following local equivalence ratio (ϕ), fuel consumption rate of (R_c), and combustion efficiency (η_c).

$$\phi = 1 + \left[\frac{1}{2}\left(\frac{X_{H2}}{X_{N2}}\right) - \left(\frac{X_{O2}}{X_{N2}}\right)\right] \bigg/ \left(\frac{B_{O2}}{B_{N2}}\right)_f \tag{2}$$

$$R_c = \left[\left(\frac{B_{O2}}{B_{N2}}\right)_f - \left(\frac{X_{O2}}{X_{N2}}\right)\right] \bigg/ \left[\left(\frac{B_{O2}}{B_{N2}}\right)_f + \left[\frac{1}{2}\left(\frac{X_{H2}}{X_{N2}}\right) - \left(\frac{X_{O2}}{X_{N2}}\right)\right]\right] \tag{3}$$

$$\eta_c = R_c \cdot \max(1,\phi) \tag{4}$$

Here, X_i is the mole fraction of species i detected by gas chromatography, and B_i is the mole fraction of species i in the vitiated air. The B_{O2}/B_{N2} ratio is constant at 0.41, as calculated from the mass flow rate of air, hydrogen and oxygen in the vitiation heater. The local ϕ included fuel consumed by combustion. The consumption rate R_c is the ratio of the amount of fuel actually burned to that of total fuel at a local point. The local η_c is the ratio of the amount of fuel actually burned to the amount available for reaction. The derivations of both ϕ and R_c see Appendix.

The uncertainties in both gas chromatography and mass flow rate yielded uncertainties in ϕ, R_c, and η_c.

$$S_\phi = \frac{|\phi - 1|}{\phi} \sqrt{\frac{1}{(X_{H2}/2X_{N2} - X_{O2}/X_{N2})^2}\left[\left(\frac{1}{2}\frac{X_{H2}}{X_{N2}}\right)^2 S_{X_{H2}}^2 + \left(\frac{X_{O2}}{X_{N2}}\right)^2 S_{X_{O2}}^2\right] + S_{X_{N2}}^2 + S_{B_{O2}}^2 + S_{B_{N2}}^2} \tag{5}$$

$$S_{R_c} = \frac{1}{R_c}\sqrt{\left(\frac{B_{O2}}{B_{N2}}\phi\right)^{-2}\left[\left(\frac{1}{2}\frac{X_{H2}}{X_{N2}}R_c\right)^2 S_{X_{H2}}^2 + \left(\frac{X_{O2}}{X_{N2}}(1-R_c)\right)^2 S_{X_{O2}}^2 + \left[\frac{X_{O2}}{X_{N2}} - R_c\left(\frac{1}{2}\frac{X_{H2}}{X_{N2}} - \frac{X_{O2}}{X_{N2}}\right)\right]^2 S_{X_{N2}}^2\right] + \left(\frac{1-R_c}{\phi}\right)^2\left[S_{B_{O2}}^2 + S_{B_{N2}}^2\right]} \tag{6}$$

$$S_{\eta_c} = S_{R_c} \quad (\phi \leq 1) \quad or \quad \sqrt{\phi^2 S_{R_c}^2 + R_C^2 S_\phi^2} \quad (\phi > 1) \tag{7}$$

The typical uncertainty in ϕ is $S_\phi = 2\%$, and that of R_c is $S_{Rc}(= S_{\eta c}) = 3\%$ at ϕ of unity. The uncertainty in R_c and η_c rapidly increases at low ϕ because the relative uncertainty in X_{H2} increases.

III.   RESULTS AND DISCUSSIONS

A. Wall-Pressure Distribution

Figure 5a plots the wall-pressure distribution using the circular injector, and Fig. 5b plots that using the stinger injector at various Φ. Here, we use P_W distributions on the opposite-side wall. The data on this wall had a few discrepancies with those on the injector-side wall typically ± 5%. Figure 5 also plots P_W distributions without fuel injection. The wall pressure without injection slowly increased in the constant-area section because of friction and decreased in the diverging section. The pressure in the diverging section was below the separation limit for the ambient pressure. The wall pressure increased from x ~ 670 mm up to the exit of the combustor because of flow separation.

For the circular injector, the combustion region was limited in the diverging section for $\Phi \leq 0.37$. For $\Phi \leq 0.37$, there were both steep increases and decreases in P_W at x ~ 50 mm in the constant-area section, but no combustion occurred there. The impingement of the bow-shock wave and the expansion waves due to the injection induced these steep changes in P_W. Jet blockage increased P_W due to the impingement of the waves. The pressure in the diverging section exceeded that without injection. These P_W distributions indicate that combustion occurred only in the diverging section for $\Phi \leq 0.37$. However, the P_W distribution at $\Phi = 0.5$ indicates that the combustion region intruded into the constant-area section. The pressure just behind the injector reached P_W/P_0 ~ 0.17, and the high-pressure around the injector remained up to the entrance of the diverging section. At $\Phi = 0.56$, the start point of the pressure rise reached the facility nozzle. The precombustion shock wave appeared far upstream of the fuel injector.

For the stinger injector, the combustion region intruded into the constant-area section for low Φ. For $\Phi \leq 0.29$, the combustion region was limited in the diverging section and intruded into the constant-area section at $\Phi = 0.38$. The pressure just downstream of the stinger injector for $\Phi = 0.38$ exceeded that of the circular injector even for $\Phi = 0.50$. The start point of the pressure rise for the stinger injector was located upstream of the injector. Only a slight change in P_W/P_0 distribution was observed when Φ increased from 0.38 to 0.50. However, a slight increase in Φ from 0.5 induced a drastic change in P_W/P_0. The precombustion shock wave intruded into the facility nozzle at $\Phi = 0.56$.

The location of the precombustion shock wave greatly affects jet penetration, because the generation of the precombustion shock wave decreases the dynamic pressure of the crossflow. We evaluated the effects of the

precombustion shock wave on J (Table 1). Here, J_∞ represents the momentum flux ratio for the undisturbed crossflow, evaluated by the incoming crossflow conditions. In addition, J_{psw} represents the momentum flux ratio at the injector position for the disturbed crossflow with the precombustion shock wave, evaluated by the mass and energy conservation laws using P_W measured at the injector position (i.e., the momentum conservation law was ignored). Density at the injector position with the precombustion shock wave was the solution of the quadratic equation delivered from the mass and energy conservations and yielded J_{psw}. Results indicate that J_{psw} for the stinger injector reached 3.8 at $\Phi \sim 0.5$. The jet penetration data in the cold flow experiments (Fig. 3) indicate that the jet penetration for the stinger injector was saturated above $J \sim 2$. Therefore, the advantage of the stinger injector for jet penetration could be lost for $\Phi \geq 0.38$, where the precombustion shock wave intrudes into the constant-area section.

B. Pressure Gain with the Stinger Injector

Figure 6 indicates the pressure gains with the stinger injector at $\Phi = 0.29$ and 0.50. The solid symbols denote the data on the injector-side wall, and the open symbols denote those on the opposite-side wall. At $\Phi = 0.29$, where the combustion region was limited in the diverging section, the pressure gain exceeded unity for the latter three-fouths of the diverging section. However, the pressure gain fell below unity for the first one-fourth of the diverging section. These data imply that combustion at the entrance of the diverging section for the stinger injector was weaker than that for the circular injector but became intensified downstream of the diverging section. At $\Phi = 0.50$, where the flame was anchored around the fuel injector, the pressure gain greatly exceeded unity around the fuel injector and remained at 1.1 in the diverging section. These data imply that combustion with the stinger injector was more intense than that with the circular injector, not only in the diverging section but also around the fuel injector.

C. Local Equivalence Ratio and Combustion Efficiency

Figure 7 presents the exit cross-sectional distributions of both the local equivalence ratio and the local combustion efficiency at $\Phi = 0.29$. The left portions of the contour maps are the data for the circular injector, and the right portions are those for the stinger injector. The dots denote the sampling points. The contour map of ϕ indicates that the jet plume of the stinger injector penetrated deeply in the vertical direction but did not spread in the lateral direction, compared with the circular injector. This trend agrees with that in the cold-flow experiment. The maximum ϕ was 1.4 for the stinger injector and 1.8 for the circular injector. The stinger injector promoted mixing between the fuel jet and the crossflow air. The contour map of η_c indicates mixing-controlled combustion for both

injectors because the minimum η_c was detected around the curve at $\phi = 1$ [28]. The minimum η_c was 0.8 for the stinger injector and 0.65 for the circular injector. The stinger injector produced high mixing and combustion efficiencies due to high jet penetration.

Figure 8 presents the contour maps of both ϕ and η_c at $\Phi = 0.5$. The contour map of ϕ indicates that the jet spreading in the lateral direction of the stinger injector was similar to that of the circular injector. However, the plume core for the stinger injector, where the highest ϕ was detected in the plume, was located nearer the injector-side wall than that for the circular injector. The plume core for the stinger injector moved toward the injector-side wall even though Φ increased from 0.29 to 0.50 (i.e., J increased from 1.56 to 2.98). The cold-flow experiment results do not explain this trend for the stinger injector.

Figure 5b indicates that the precombustion shock wave existed across the stinger injector at $\Phi = 0.50$. The structure of the shock train probably dominated the jet penetration of the stinger injector. A pseudo-shock wave contains some bifurcated shock waves and boundary-layer separations [29]. The injectant preferentially spread within the low momentum flux region near the wall including the separation bubbles. In addition, the foot of the bifurcated shock wave probably impinged into the jet, resulting in the deflection of the plume toward the injector-side wall, as demonstrated in the experiments conducted by Schetz et al. [30].

The precombustion shock wave restricted vertical penetration of fuel for the stinger injector, but it promoted lateral spreading of the fuel. The maximum ϕ was lower than that for the circular injector even at $\Phi = 0.50$. The lateral spreading of fuel due to the precombustion shock wave promoted mixing of the fuel jet and the crossflow air. The minimum η_c was detected around the curve at $\phi = 1$ for both injectors. Therefore, at the exit plane, the mixing rate of fuel controlled combustion even at $\Phi = 0.50$. The minimum ϕ was 0.8 for the stinger injector and 0.65 for the circular injector. The stinger injector still produced higher combustion efficiency than the circular injector. The high combustion efficiency of the stinger injector explains the pressure measurements at $\Phi = 0.5$.

We remapped ϕ and η_c contoured distributions as a $\phi - R_c$ diagram. Figure 9a presents the data for $\Phi = 0.29$, and Fig. 9b presents that for $\Phi = 0.50$. The solid symbols and solid lines in each figure represent the data for the stinger injector. The open symbols and dashed lines represent the data for the circular injector. Figure 9 also represents the data near the injection wall by the special symbols and the broken lines. These figures indicate why the stinger injector produced higher P_W than the circular injector in the diverging section for both Φ's.

Figure 9a indicates that the stinger injector produced large-scale mixing due to higher jet penetration and promoted fine-scale mixing and combustion except near the wall at $\Phi = 0.29$. The maximum ϕ for the stinger injector was 1.5, which was much lower than the maximum for the circular injector. Thus, the stinger injector promoted large-scale mixing than the circular injector. For the stinger injector, the initial penetration near the fuel injector was much higher than that for the circular injector [25]. The plume from the stinger injector more fully contacted the high-speed crossflow air, promoting the development of a shear layer with large eddies around the jet. As a result, the maximum ϕ of the stinger injector became lower than that of the circular injector.

R_c for the stinger injector was much higher than that for the circular injector at a given ϕ. Thus, the stinger injector promoted fine-scale mixing, leading to better combustion. A mixing transition occurs at a high Reynolds number, and finer structures were generated within larger structures [31]. For the stinger injector, many fine structures were generated within the larger eddies, because the contact area between the jet and the crossflow air exceeded that of the circular injector.

In contrast, the data near the wall for the stinger injector coincided with those for the circular injector. The intense disturbance and the low velocity within the boundary layer promoted both mixing and combustion in this region. Therefore, the difference in injector shape was insignificant for mixing and combustion.

Figure 9b indicates that the superiority of the stinger injector over the circular injector decreased at $\Phi = 0.50$. However, the data for the stinger injector still indicates that the stinger injector promoted both large- and fine-scale mixing slightly more than the circular injector did. We believe that this was due to the precombustion shock wave in front of the fuel injector. The precombustion shock wave disturbed the crossflow and promoted mixing close to the injector. In addition, it recovered the pressure and temperature, and promoted combustion close to the injector. Separation with the precombustion shock wave provided a longer residence time for the fuel. These phenomena compensated for the decreased mixing and combustion efficiencies due to the reduced jet penetration for the stinger injector.

One reason the stinger injector easily produced a precombustion shock wave seems to be its better flame-holding. Figure 10 presents heat marks around the injectors at $\Phi = 0.5$ for the circular injector (Fig. 10a) and for the stinger injector (Fig. 10b). We took these pictures after operating the wind tunnel seven times under the same conditions. The surfaces were polished before the first test run.

Figure 10a indicates that copper rust (white region) formed on the surface around the circular injector with combustion. Intense combustion occurred near the wall and was limited behind the detached bow shock wave. A very intense heat mark formed behind the reattachment shock. In contrast, Fig. 10b does not indicate an intense heat mark on the surface around the stinger injector. Only bow shock due to the injection could be observed. The bow-shock wave for the stinger injector was very close to the leading edge of the injector. This is evidence that the stinger injector reduced total pressure loss; thus, the stinger injector produced high P_W in the diverging section.

No flame-holding region was observed near the wall of the stinger injector, but the wall pressure around the stinger injector was higher than that around the circular injector. The flame-holding region was probably detached from the wall. Srinivasan et al. [17] reported a lateral vortex pair at the trailing edge of the diamond-shaped injector, and this vortex pair had the potential to hold flame. A similar vortex likely occurred in the stinger injector, and flame should be anchored in the vortex. Figure 10b indicates that the bow shock for the stinger injector expanded in the rear half of the injector. This is evidence of a pressure rise with combustion behind the injector. We believe the detached vortex pair anchored the flame and increased the pressure behind the injector. The mechanisms of the flame-holding for the stinger injector will be investigated in future work.

D. Increment of Pressure Integration

Figure 11 summarizes the increment of pressure integration for the stinger and circular injectors. The solid symbols denote the data for the stinger injector, and the open symbols denote the data for the circular injector. The vertical axis denotes the thrust coefficient with combustion as mentioned previously, and the horizontal axis denotes Φ. We can classify the data into three categories by thrust level and its sudden change. The first change in ΔF occurred when the combustion region reached the diverging section, and the flame anchoring point jumped to the region around the injector. The second change in ΔF occurred when the precombustion shock wave jumped from near the injector to the exit of the facility nozzle. Based on this data, this trend in the stinger injector data is similar to that in the circular injector data. The increment of pressure integration for the stinger injector, however, was higher than that for the circular injector for $\Phi \leq 0.55$. In addition, the transition Φ where ΔF steeply changed was lower than those for the circular injector. This was further evidence that the stinger injector produced more intense combustion than the circular injector.

For $\Phi > 0.55$, the precombustion shock wave was located far upstream of the fuel injector. Here the shape of the injector did not affect thrust performance. When the precombustion shock wave appeared far upstream of the fuel

injector, the dynamic pressure of the disturbed crossflow decreased and its disturbance greatly increased, due to the shock wave and the separation of the boundary layer. As a result, the mixing and combustion of the fuel were promoted, and the difference in injector shape was insignificant for combustor performance.

IV.   CONCLUSION

A stinger injector with a sharp leading edge in front of a stream-wise slit was applied in a Mach 2.44 supersonic combustor with a 1.66° diverging section at a stagnation temperature of 2060 K. Wall pressure and gas sampling measurements confirmed the ability of the stinger injector to function as a supersonic combustor. The measured data were compared with those of a conventional circular injector, and the following conclusions were obtained.

1) Stinger injection produced greater jet penetration in the height-wise direction, as expected from the results of a cold-flow experiment, when the combustion region was limited in the diverging-area combustor for $\Phi < 0.3$. Greater jet penetration produced large eddies with a shear layer between the fuel jet and high-speed crossflow air, which promoted fine-scale mixing and combustion, resulting in 10% greater pressure thrust than for the circular injector.

2) At $\Phi = 0.5$, a precombustion shock wave occurred just in front of the stinger injector but behind the circular injector. The precombustion shock just in front of the injector restricted the vertical penetration of the jet. For the stinger injector, the plume core moved toward the injection wall, though the momentum flux ratio increased.

3) When the flame was anchored around the injector, the stinger injector produced much greater wall pressure around the injector than the circular injector did. In addition, it produced 10% greater pressure thrust in the diverging-area combustor than the circular injector, though its vertical penetration was less than that of the circular injector. Mixing enhancement due to the precombustion shock in front of the stinger injector and better flame-holding of the injector resulted in greater pressure thrust.

4) Once a precombustion shock wave formed far upstream of the fuel injector, injector-port shape had no insignificant impact on combustor performance, because the precombustion shock wave drastically increased the jet-to-crossflow momentum flux ratio and the turbulence of the crossflow air. As a result, the stinger injector produced a pressure thrust similar to that of the circular injector even in a high momentum flux ratio regime, where the penetration of the stinger injector was poorer than that of the circular injector in the cold-flow experiments.

Thus, the stinger injector achieved a pressure thrust greater than or equal to that of circular injector at all fuel equivalence ratios. This work confirmed that the stinger injector yielded high combustor performance as a supersonic combustor.

APPENDIX

Derivation of Fuel Consumption rate and Local Equivalence Ratio: The fuel consumption rate R_c is the ratio of the amount of fuel actually burned to that of total fuel at a local point. This definition yields $R_c = (n_{H2}-n'_{H2})/n_{H2}$, where n_i is molar concentration of species i at a sampling point before combustion, and n'_i is that after combustion. The molar concentration of each species after combustion can be written by using R_c and n_{H2}:

$$
\begin{aligned}
n'_{N2} &= n_{N2} \\
n'_{O2} &= n_{O2} - \frac{1}{2}R_c n_{H2} \\
n'_{H2} &= n_{H2} - R_c n_{H2} \\
n'_{H2O} &= n_{H2O} + R_c n_{H2}
\end{aligned}
\tag{A1}
$$

The measured mole fraction of species i is $X_i = n'_i/(n'_{N2}+n'_{O2}+n'_{H2})$, because our gas chromatography cannot detect H_2O. On the other hand, the mole fraction of species i in the vitiated crossflow-air is $B_i = n_i/(n_{N2}+n_{O2}+n_{H2O})$. From these equations and Eq. A1, we obtain the formulae as follows:

$$
\frac{X_{O2}}{X_{N2}}\left(=\frac{n'_{O2}}{n'_{N2}}\right) = \frac{B_{O2}}{B_{N2}} - \frac{1}{2}R_c\frac{n_{H2}}{n_{N2}}
\tag{A2}
$$

$$
\frac{X_{H2}}{X_{N2}}\left(=\frac{n'_{H2}}{n'_{N2}}\right) = \left(1-R_c\right)\frac{n_{H2}}{n_{N2}}
\tag{A3}
$$

Eliminating n_{H2}/n_{N2} from Eq. A2 and A3, we obtain the consumption rate R_c:

$$
R_c = \left[\left(\frac{B_{O2}}{B_{N2}}\right)_f - \left(\frac{X_{O2}}{X_{N2}}\right)\right] \Big/ \left[\left(\frac{B_{O2}}{B_{N2}}\right)_f + \left[\frac{1}{2}\left(\frac{X_{H2}}{X_{N2}}\right) - \left(\frac{X_{O2}}{X_{N2}}\right)\right]\right]
\tag{A4}
$$

Local equivalence ratio ϕ is defined as $\phi = 1/2\, n_{H2}/n_{O2}$, which includes fuel consumed by combustion. Dividing n'_{O2} by n'_{H2}, we obtain the formula A5:

$$
\frac{X_{O2}}{X_{H2}}\left(=\frac{n'_{O2}}{n'_{H2}}\right) = \frac{1}{2\left(1-R_c\right)}\left(\frac{1}{\phi}-R_c\right)
\tag{A5}
$$

Substituting Eq. R3 into Eq. R4, we obtain the local equivalence ratio:

$$\phi = 1 + \left[\frac{1}{2} \left(\frac{X_{H2}}{X_{N2}} \right) - \left(\frac{X_{O2}}{X_{N2}} \right) \right] \bigg/ \left(\frac{B_{O2}}{B_{N2}} \right)_f \tag{A6}$$

References

[1] Mitani, T., Tomioka, S., Kanda, T., Chinzei, N., and Kouchi, T., "Scramjet Performance Achieved in Engine Tests from M4 to M8 Flight Conditions," *AIAA paper 2003-7009*, 2003.

[2] Seiner, J. M., Dash, S. M., and Kenzakowski, D. C., "Historical Survey on Enhanced Mixing in Scramjet Engines," *Journal of Propulsion and Power*, Vol. 17, No. 6, 2001, pp. 1273-1286. [DOI: 10.2514/2.5876]

[3] Northam, G. B., Greenberg, I., Byington, C. S., and Capriotti, D. P., "Evaluation of Parallel Injector Configurations for Mach 2 Combustion," *Journal of Propulsion and Power*, Vol. 8, No. 2, 1992, pp. 491–499. [DOI:10.2514/3.23503]

[4] Donohue, J.M., McDaniel, J.C. and Haj-Hariri, H., "Experimental and Numerical Study of Swept Ramp Injection into a Supersonic Flowfield," *AIAA Journal*, Vol. 32, No. 9, 1994, pp. 1860-1867. [DOD: 10.2514/3.12184]

[5] Siebenhaar, A., Bulman, M.J., and Bonnar, D.K., "Strutjet Rocket-Based Combined-Cycle Engine," *Progress in Astronautics and Aeronautics*, Vol. 189, pp. 697-755.

[6] Gruber, M. R., Carter, C. D., Montes, D. R., Haubelt, L. C., King, P. I., and Hsu, K.-Y., "Experimental Studies of Pylon-Aided Injection into a Supersonic Crossflow," *Journal of Propulsion and Power*, Vol. 24, No. 3, 2008, pp. 460–470. [DOI:10.2514/1.32231]

[7] Takahashi, H., Tu, Q., and Segal, C., "Effects of Pylon-Aided Fuel Injection on Mixing in a Supersonic Flowfield," *Journal of Propulsion and Power*, Vol. 26, No. 5, 2010. [DOI: 10.2514/1.48393]

[8] Kouchi, T., Hoshino, T., Sasaya, K., and Masuya, G., "Time-Space Trajectory of Unsteady Jet into Supersonic Crossflow Using High-Speed Framing Schlieren Images," *AIAA paper 2009-7316*, 2009.

[9] Billig, F.S., Orth, R.C., and Lasky, M., "A Unified Analysis of Gaseous Jet Penetration," *AIAA Journal*, Vol. 9, No. 6, 1971, pp. 1048-1057. [DOI: 10.2514/3.49916]

[10] Mays, R. B., Thomas, R. H., and Schetz, J. A., "Low Angle Injection into a Supersonic Flow," AIAA189-2461, 1989

[11] Gruber, M. R., Nejad, A. S., Chen, T. H., and Dutton, J. C., "Mixing and Penetration Studies of Sonic Jets in a Mach 2 Freestream," *Journal of Propulsion and Power*, Vol. 11, No. 2, 1995, pp. 315-323.

[12] Bowersox, R. D. W., "Turbulent Flow Structure Characterization of Angled Injection into a Supersonic Crossflow," *Journal of Propulsion and Power*, Vol. 34, No. 2, 1997, pp. 205–213. [DOI: 10.2514/2.3194]

[13] Gruber, M. R., Nejad, A. S., Chen, T. H., and Dutton, J. C., "Transverse Injection from Circular and Elliptic Nozzles into a Supersonic Crossflow," *Journal of Propulsion and Power*, Vol.16 No.3, 2000, pp. 449-457. [DOI: 10.2514/2.5609]

[14] Barber, M., Schetz, J.A., and Roe, L.A., "Normal, Sonic Helium Injection Through a Wedge-Shaped Orifice into Supersonic Flow," *Journal of Propulsion and Power*, Vol. 13, No. 2, 1997, pp. 257-263. [DOI: 10.2514/2.5157]

[15] Tomioka, S., Jacobsen, L. S. and Schetz, J. A., "Sonic Injection from Diamond-Shaped Orifices into a Supersonic Crossflow ," *Journal of Propulsion and Power*, Vol. 19, No. 1, 2003, pp. 104-114. [DOI: 10.2514/2.6086]

[16] Kobayashi, K., Bowersox R., Srinivasan, R., Carter, C., and Hsu, K.-Y., "Flowfield Studies of Diamond-Shaped Fuel Injector in a Supersonic Flow," *Journal of Propulsion and Power*, Vol.23 No.6, 2007, pp. 1168-1176.

[17] Srinivasan, R., and Bowersox, R., "Simulation of Transverse Gaseous Injection Through Diamond Ports into Supersonic Freestream ," *Journal of Propulsion and Power,* Vol. 23, No. 4, 2007, pp. 772-782. [DOI: 10.2514/1.18405]

[18] Schetz, J. A., Maddalena, L., Throckmorton, R., and Neel, R., "Complex Wall Injector Array for High-Speed Combustors," *Journal of Propulsion and Power*, Vol. 24, No. 4, 2008, pp. 673–680. [DOI:10.2514/1.36660]

[19] Fuller, R. P., Wu, P.-K., Nejad, A. S., and Schetz, J. A., "Comparison of Physical and Aerodynamic Ramps as Fuel Injectors in Supersonic Flow", *Journal of Propulsion and Power*, Vol. 14, No. 2, 1998, pp. 135-145.

[20] Eklund, D. R, Fletcher, D. G., Hartfield Jr, R. H., McDaniel, J. C., Northam, G. B., Dancey, C. L., and Wang, J. A., "Computational/Experimental Investigation of Staged Injection into a Mach 2 Flow," AIAA Journal, Vol. 32, No. 5, 1994, pp. 907-916.

[21] Cox-Stouffer, S. K., G r u b e r, M. R., and Bulman, M. J., "A Streamlined, Pressure-Matched Fuel Injector for Scramjet Applications," AIAA 2000-3707, 2002

[22] Meicenheimer, H. L., Gutmark, E. J., Carter, C. D., Eklund, D. R., Gruber, M. R., Hsu, K.–Y., "Independent Stage Control of a Cascade Injector," AIAA 2005-3708, 2003.

[23] Tomioka, S., Izumikawa, M., Kouchi, T., Masuya, G., Hirano, K., and Matsuo, A., "Matched Pressure Injections into a Supersonic Crossflow through Diamond-Shaped Orifices," *Journal of Propulsion and Power,* Vol. 24, No. 3, 2008, pp. 471-478. [DOI: 10.2514/1.35177]

[24] Tomioka, S., Kouchi, T., Masumoto, R., Izumikawa, and Matsuo, A., "Supersonic Combustion with Supersonic Injection Through Diamond-Shaped Orifices," *Journal of Propulsion and Power,* Vol. 27, No. 6, 2011, pp. 1196-1203. [DOI: 10.2514/1.B34164]

[25] Hirano, K. Matsuo, A., Kouchi, T., Tomioka, S., Izumikawa, M., "New Injector Geometry for Penetration Enhancement of Perpendicular Jet into Supersonic Flow," *AIAA paper* 2007-5028, 2007.

[26] Rogers, R. C., Mixing of Hydrogen Injected from Multiple Injectors Normal to a Supersonic Airstream," NASA TN D-6476, 1971.

[27] Billigs, F. S., "Research on Supersonic Combustion," *J. Prop. and Power*, Vol. 9, No. 4, 1993, 499-514. [DOI: 10.2514/3.23652]

[28] Mitani, T., Chinzei, N., and Kanda, T., "Reaction and Mixing-Controlled Combustion in Scramjet Engines," *J. Prop. and Power*, Vol. 17, No. 2, 2001, pp. 308-314. [DOI: 10.2514/2.5743]

[29] Matsuo, K., Miyazato, Y., and Kim, H.-D., "Shock Train and Pseudo Shock Phenomena in Internal Gas Flows," *Progress in Aerospace Sciences*, Vol. 35, 1999, pp. 33-100.

[30] Schetz, J., Maddalena, L., Burger, S., "Molecular Weight and Shock-Wave Effects on Transverse Injection in Supersonic Flow;" Journal of Propulsion and Power, Vol. 26, No. 5, 2010, pp. 1102-1113. [DOI: 10.2514/1.49355]

[31] Dimotakis, P.E., "The mixing transition in turbulent flows," *J. Fluid Mech.,* vol. 409, 2000, pp. 69–98.
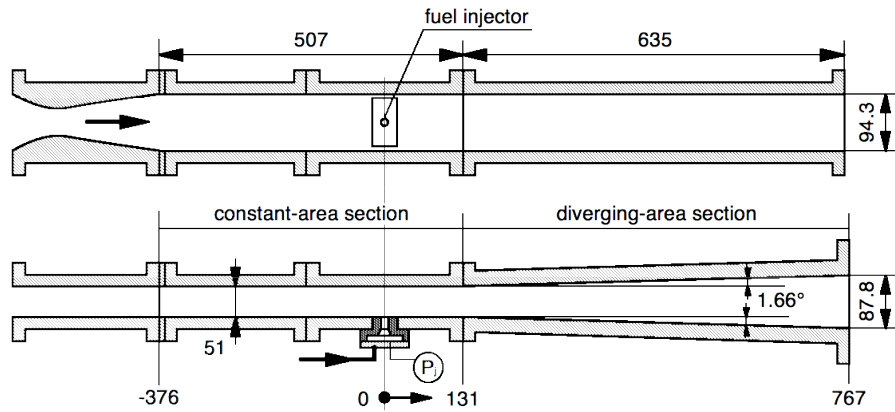
Fig. 1. Schematic diagram of supersonic combustor.
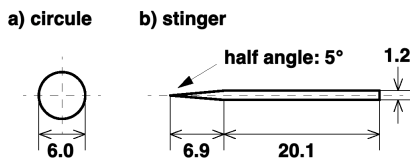
Fig. 2. Schematic diagram of fuel injection orifices. Fuel is injected in the direction perpendicular to the paper, while crossflow air comes left to right.
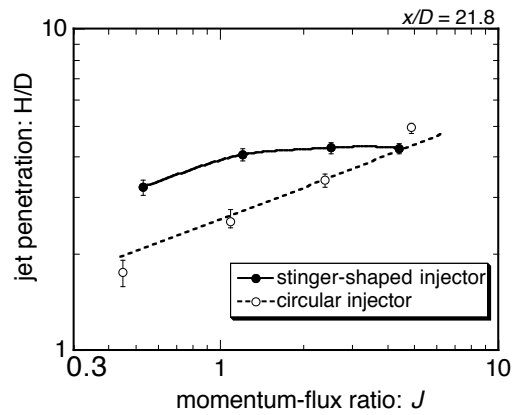
Fig. 3. Jet penetration as a function of momentum-flux ratio using stinger-shaped injector, compared with that using circular injector.
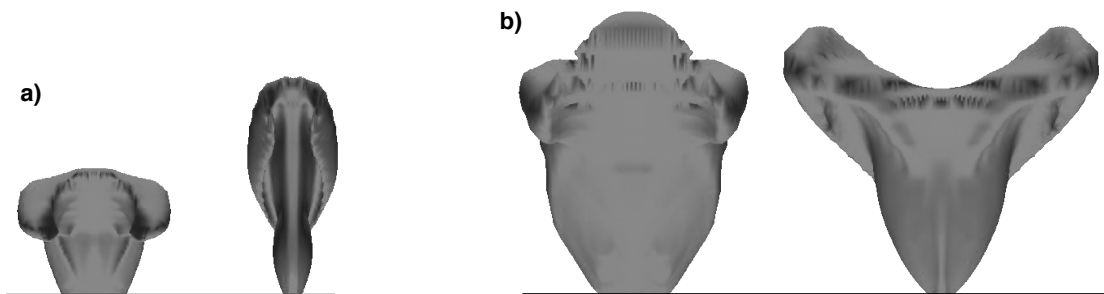
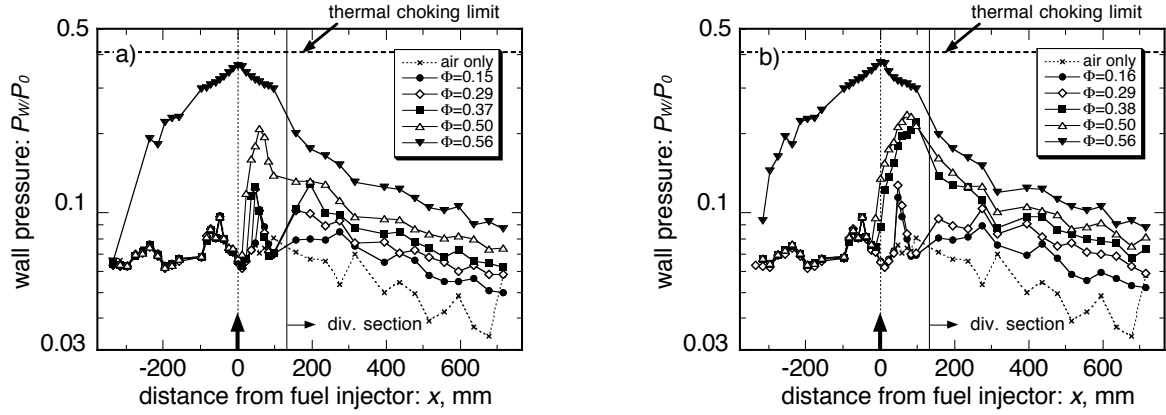**Fig. 4. Computed plume shapes using circular (left) and stinger-shaped (right) injectors: (a) $J = 1$ and (b) $J = 4$ [25].**

Fig. 5. Wall pressure distributions using (a) a circular injector and (b) a stinger-shaped injector at various Φ.

Table 1.   Momentum flux ratio at various Φ

	circular				stinger		
Φ	J_∞	J_{psw}	J_{psw}/J_∞	Φ	J_∞	J_{psw}	J_{psw}/J_∞
0.15	0.77	-	1.00	0.16	0.88	-	1.00
0.29	1.51	-	1.00	0.29	1.56	-	1.00
0.37	1.89	-	1.00	0.38	2.12	2.42	1.14
0.50	2.52	-	1.00	0.50	2.66	3.80	1.43
0.56	2.90	9.11	3.14	0.56	3.05	9.79	3.21
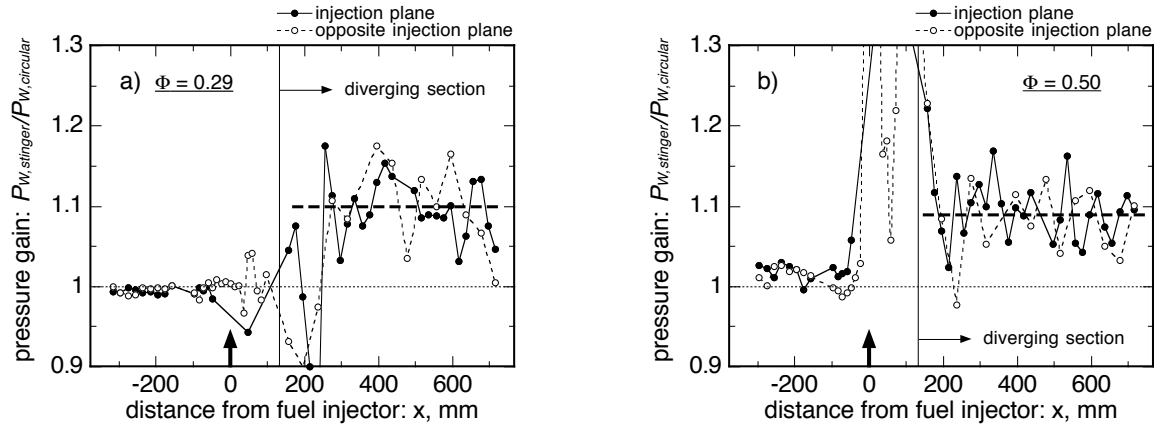
Fig. 6. Pressure gain with stinger-shaped injector at (a) $\Phi = 0.29$ and (b) $\Phi = 0.5$.

20
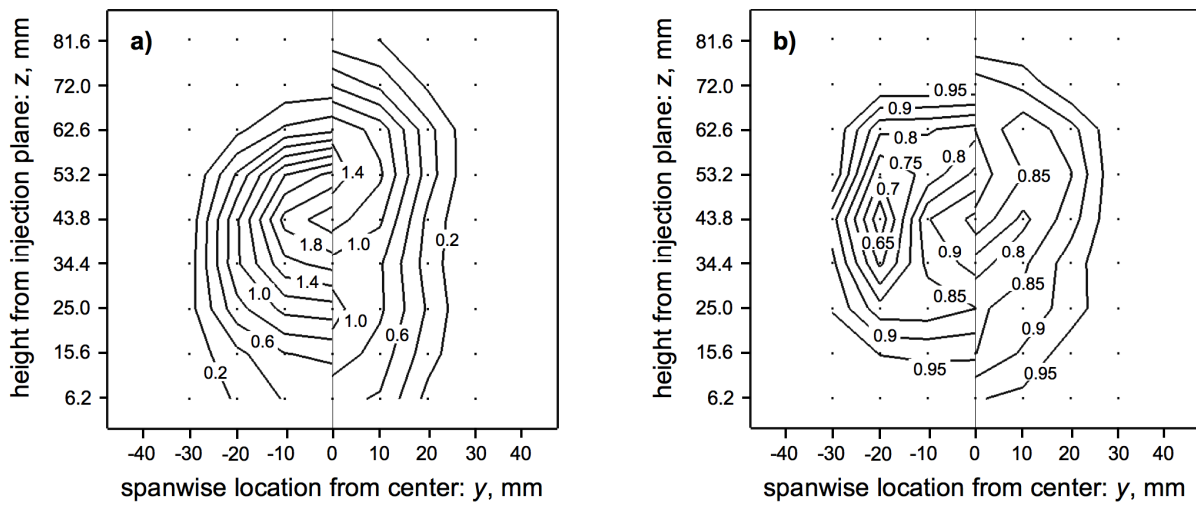
Fig. 7. Distributions of (a) local equivalence ratio and (b) combustion efficiency at the exit of combustor with a circular injector (left) and a stinger-shaped injector (right) at $\Phi = 0.29$.
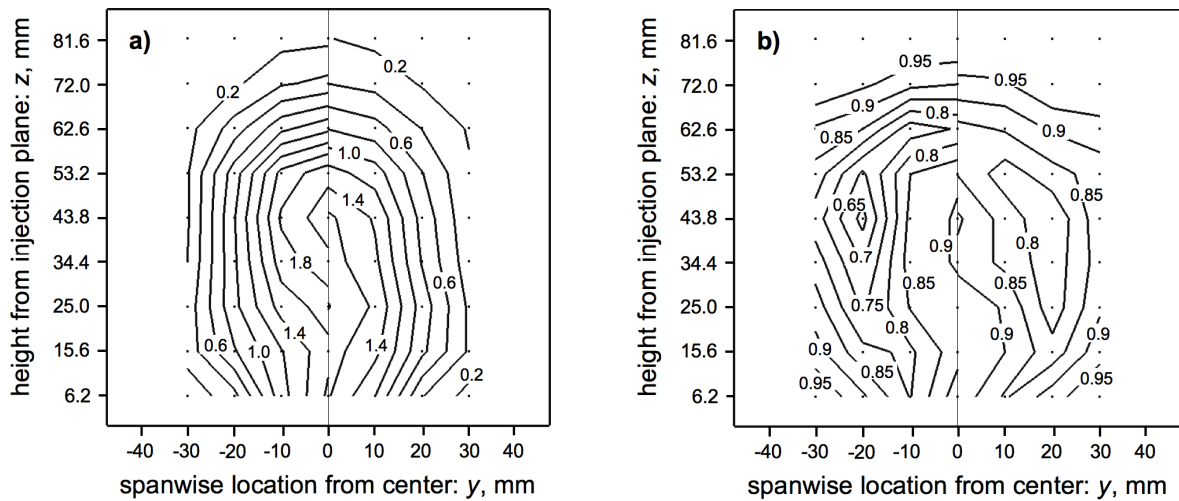
Fig. 8. Distributions of (a) local equivalence ratio and (b) combustion efficiency at the exit of combustor with a circular injector (left) and a stinger-shaped injector (right) at $\Phi = 0.50$.
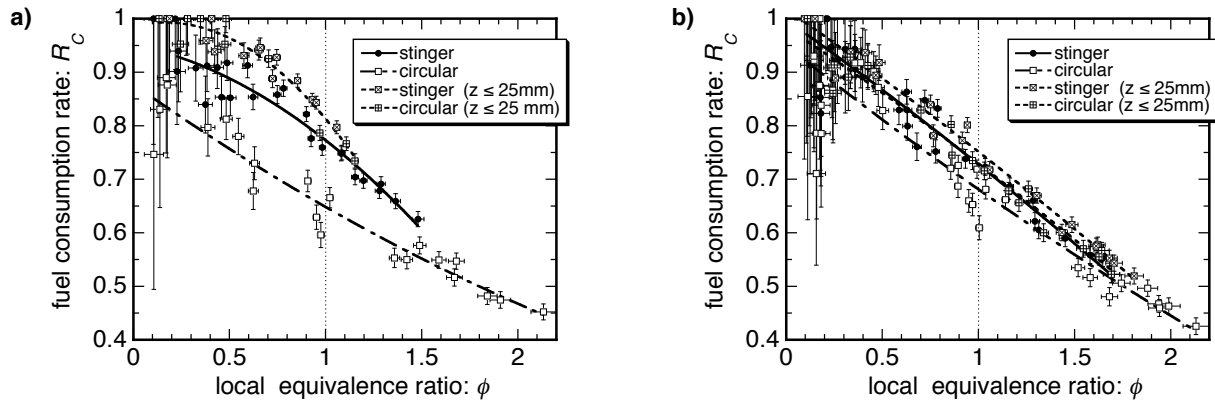
Fig. 9. Fuel consumption ratio as a function of local equivalence ratio at (a) $\Phi = 0.29$ and (b) $\Phi = 0.50$.
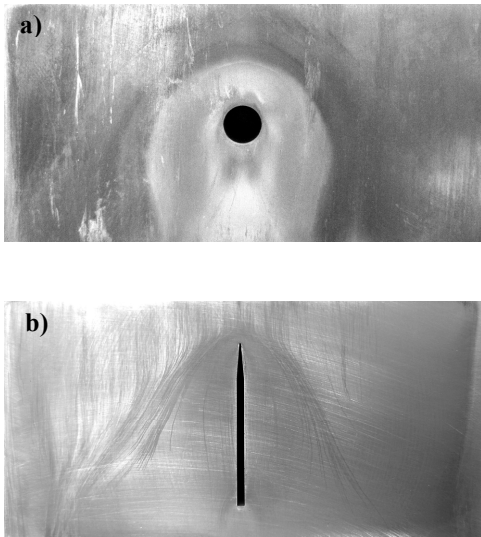

Fig. 10. Heat marks around (a) circular and (b) stinger-shaped injectors at $\Phi = 0.5$.
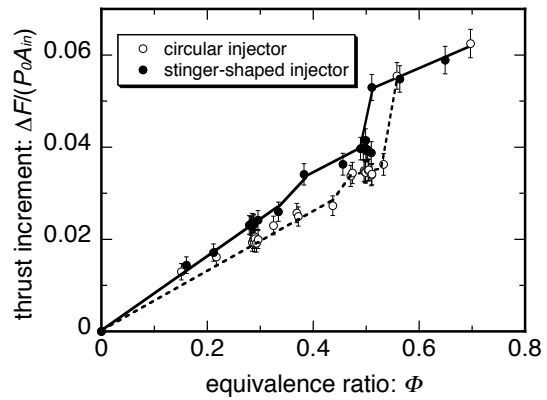

Fig. 11   Increment of pressure integration due to combustion with a stinger-shaped injector, compared with that with a circular injector.